

Materials made available here are subject to the IEEE copyright policy. Find policy here:
<http://iee.org>

By choosing to view this document, you agree to fulfill all of your obligations with respect to IEEE-copyrighted material.

The publication can be found at the following URL on the IEEE website:
http://ieeexplore.ieee.org/xpl/freeabs_all.jsp?arnumber=1504763

Dynamic High-Pressure Calibration of the Fiber-Optic Sensor Based on Birefringent Side-Hole Fibers

Magdalena S. Nawrocka, Wojtek J. Bock, *Fellow, IEEE*, and Wacław Urbanczyk

Abstract—This paper presents a dynamic pressure calibration of the fiber-optic interferometric sensor based on highly birefringent side-hole fibers. Earlier, we tested other types of fiber-optic sensors based on the same principle for measurements of static and quasi-static pressure. To apply the sensor for measurements of fast pressure changes, the dynamic analysis is crucial due to the occurrence of resonance phenomena and due to the possibility of false pressure readings. We applied a static calibration procedure to initially determine the pressure sensitivity and temperature stability of the sensor. Next, we compared the characteristics of the fiber-optic sensor with the responses of a calibrated piezoelectric dynamic pressure sensor at an operating range of 110 bar with a sampling rate equal to 200 kHz. The characteristics of the fiber-optic sensor are in good agreement with those of the reference piezoelectric sensor for the linear and exponential functions and for the half-sine when the pulse is wider than 400 ms. However, for half-sine pulses narrower than 250 ms, resonance oscillations occur only in the reference sensor. Construction of the fiber-optic sensor reduces the undesirable oscillations, which thereby makes it possible to operate on frequencies higher by about one order than in the case of the piezoelectric sensor. It clearly shows that the highly birefringent fiber-optic sensors can be successfully applied for measurements of rapid pressure changes.

Index Terms—Dynamic pressure, fiber-optic sensor, highly birefringent fiber, side-hole fiber.

I. INTRODUCTION

THE most important advantage of optical fibers used for sensing applications is that the information is carried by light. Hence, in contrast to conventional electronic devices, fiber-optic sensors can be applied in the presence of high electromagnetic interference. Moreover, the optical signal does not generate sparks; thus, in addition to transferring data over a long distance, fiber-optic sensors can be applied in harsh environments.

Manuscript received February 11, 2004; revised July 8, 2004. This work was supported by the NSERC and NATEQ, Canada. The associate editor coordinating the review of this paper and approving it for publication was Prof. Ewald Benes.

M. S. Nawrocka was with the Centre de Recherche en Photonique, Département d'Informatique et d'Ingénierie, Université du Québec en Outaouais, QC J8X 3X7, Canada, and is now with Department of Electrical and Computer Engineering, Florida International University, Miami, FL 33174 USA (e-mail: nawrocka@fiu.edu)

W. J. Bock is with the Centre de Recherche en Photonique, Département d'Informatique et d'Ingénierie, Université du Québec en Outaouais, QC J8X 3X7, Canada (e-mail: wojtek.bock@uqo.ca)

W. Urbanczyk is with the Institute of Physics, Wrocław University of Technology, 50-370 Wrocław, Poland (e-mail: urban@if.pwr.wroc.pl).

Digital Object Identifier 10.1109/JSEN.2005.845190

Fiber-optic sensors have been explored for measurements of diverse parameters [1], [2]. A survey of recent literature shows that numerous applications require dynamic pressure measurements, in fields such as automotive engineering, aerodynamics, acoustics, fluid control, blast waves, and medicine [3], [4]. Static and quasi-static calibration is not sufficient for sensors that are called on to test rapidly changing measurands. The dynamic behavior of the sensor is different from its static characteristic, especially if a measurand changes with a frequency that results in resonance phenomena. To determine the real potential of the sensor for applications involving fast changing parameters, its dynamic behavior must be carefully investigated.

Many efforts have been directed to establishing methods for dynamic pressure calibration. However, although primary standards exist for a wide range of static pressure, primary dynamic pressure calibration service is directed mostly to acoustic measurements, which are characterized by low-amplitude pressure. In this paper, we are proposing to extend the focus to calibration of high-amplitude dynamic pressure sensors, which requires a different approach than those used in acoustics. Various methods for generating both periodic and nonperiodic dynamic pressure have been studied. In practice, it is easier to produce single-event pressure pulses than periodic pressure signals, especially when high-pressure amplitudes are required. One of the simplest techniques for achieving a pressure pulse resembling the half-sine of a time interval of the order 10 ms is the dropping weight method. A falling object hits a piston that acts on a pressure transducer through a volume of oil. However, the main disadvantage is that the pressure generated in this way cannot be determined precisely, and, thus, a reference pressure sensor is required. Another easy way to achieve a negative-pressure step pulse is to apply a fast opening valve, which makes it possible to change the pressure from maintained value to atmospheric pressure. The amplitude of the pressure can be monitored precisely using the primary static pressure standard; however, the drop time is of the order of hundreds of milliseconds, which is much longer than the pulses from the dropping-weight generator. Another disadvantage is that it is impossible to obtain an ideal step pulse; thus, the load pressure should in fact be considered as an exponentially decaying pressure change. During the dynamic calibration, it is reasonable to adjust the profile of the pressure signal to the actual measurement situation if at all possible. If a pressure sensor is intended for application in different measurement situations, it follows logically that the sensor should be tested using different pressure functions.

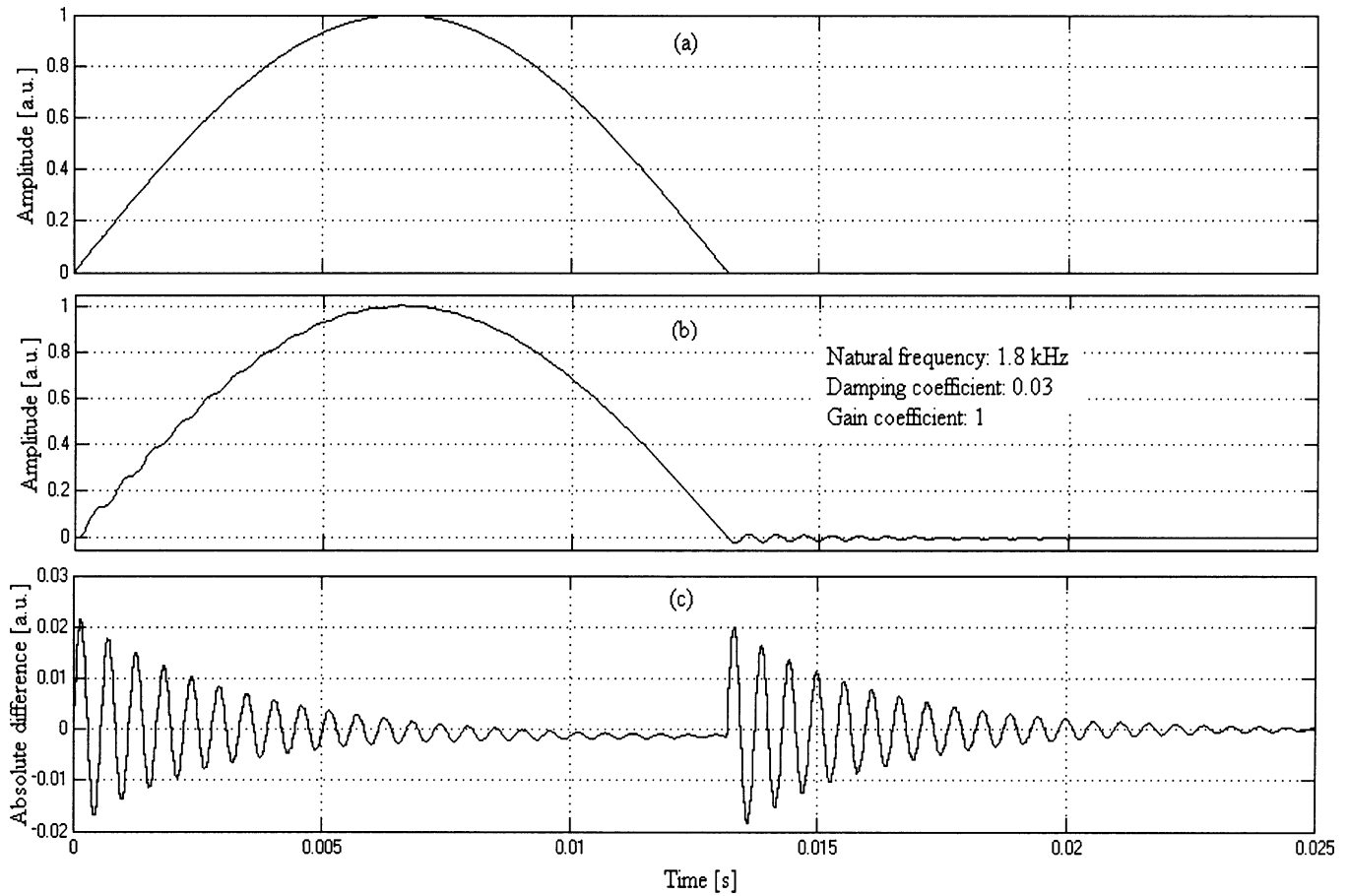


Fig. 1. Theoretical response of the second-order transducer to the half-sine pulse. (a) Half-sine input function with a time interval of 13 ms. (b) Response of the transducer with a natural frequency of 1.8 kHz, damping and gain coefficient equal to 0.03 and 1, respectively. (c) Absolute difference between the input function and the transducer's response.

Highly birefringent (HB) fibers have been widely tested in pressure measurements [5], [6]. However, fast compression and decompression processes are associated with the temperature changes. It is well known that HB fibers are sensitive to pressure as well as to temperature. The HB fibers used most often have a maximum pressure-to-temperature sensitivity ratio equal to 0.2 °C/bar. Therefore, pressure sensors employing such fibers require temperature compensation, which has been accomplished by adding an additional fiber in a differential configuration [7]. We took advantage of the unique properties of a side-hole fiber to assure minimum sensitivity to temperature effects [8]. The side-hole fibers, having two air channels positioned in proximity to their elliptical core [9], show exceptionally high sensitivity to hydrostatic pressure and are characterized by a very high pressure-to-temperature sensitivity ratio (up to 25 °C/bar), which is about two orders of magnitude higher than in the case of other HB fibers. In contrast to other HB fiber-optic pressure sensors, the sensor presented in the paper requires no additional temperature-compensating fiber, thus avoiding degradation of the intensity and contrast of the sensor signal [10] and keeping the technology process straightforward. Testing of side-hole fibers has focused primarily on their use for the measurement of low pressures, not exceeding 25 bar [6], [11]. We show that side-hole fibers

can be applied to measurements of higher dynamic pressures at an operating range of 110 bar.

II. THEORETICAL DYNAMIC RESPONSE OF PRESSURE TRANSDUCER

The simplest and best known model of pressure sensor is a linear second-order transducer, which is described by a linear second-order differential equation with constant mass m , stiffness k , and viscous damping c , as follows:

$$F(t) = m \frac{d^2x(t)}{dt^2} + c \frac{dx(t)}{dt} + kx(t) \quad (1)$$

where $F(t)$ is the external force causing a pressure change. The well-known form of this equation, which is convenient for vibration analysis, is expressed in the following way:

$$\frac{F(t)}{m} = \frac{d^2x(t)}{dt^2} + 2\xi\omega_n \frac{dx(t)}{dt} + \omega_n^2 x(t). \quad (2)$$

Here, ω_n is a natural frequency of the transducer, whereas ξ is a relative damping factor and c_c is a critical damping

$$\omega_n = \sqrt{\frac{k}{m}}, \quad \xi = \frac{c}{c_c} = \frac{c}{2m\omega_n}. \quad (3)$$

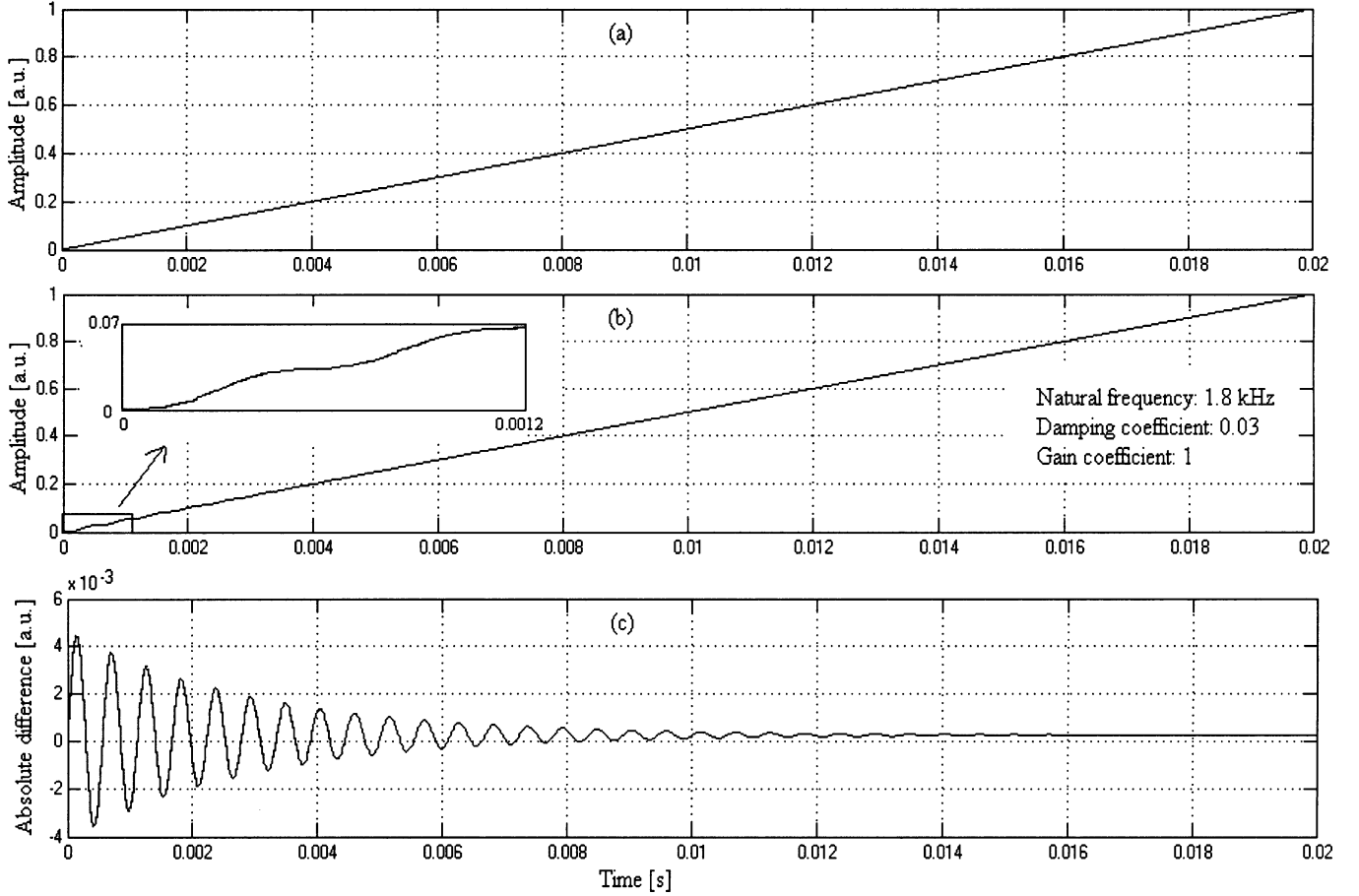


Fig. 2. Theoretical response of the second-order transducer to the linear function. (a) Input function with a slope of 50 a.u./s. (b) Response of the transducer with a natural frequency of 1.8 kHz, damping and gain coefficient equal to 0.03 and 1, respectively. (c) Absolute difference between the input function and the transducer's response.

The general solution for (2) with the initial conditions $x(0) = x_0$ and $dx(0)/dt = v_0$ is expressed as follows [12]:

$$\begin{aligned}
 x(t) &= \frac{1}{m\omega_d} \int_0^t F(\tau) e^{-\xi\omega_n(t-\tau)} \sin\omega_d(t-\tau) d\tau \\
 &+ e^{-\xi\omega_n t} \left(\frac{x_0}{\sqrt{1-\xi^2}} \cos(\omega_d t - \psi) + \frac{v_0}{\omega_d} \sin\omega_d t \right) \\
 \psi &= \tan^{-1} \frac{\xi}{\sqrt{1-\xi^2}}
 \end{aligned} \quad (4)$$

with the damped vibration frequency ω_d defined as

$$\omega_d = \omega_n \sqrt{1 - \xi^2}. \quad (5)$$

The first part of (4), which is expressed by the integral, is the response to external force, and the second part is the response dependent on initial conditions. For simple input functions, such as unit impulse, unit step, or linear function, it is easy to find the analytical expression of a transducer response, whereas for more general functions, e.g., a half-sine pulse, the transducer response must be solved numerically. Figs. 1–3 present examples of responses to half-sine pulse, step and linear functions with different natural frequencies, and damping factors. These examples are similar to the test results presented in this paper.

III. EXPERIMENTAL SETUP

The tested fiber-optic sensor and the reference piezoelectric sensor are connected in a parallel configuration to the KISTLER drop-weight dynamic pressure generator, which produces half-sine pressure pulses that act simultaneously on the two sensors, as shown in Fig. 4. Both sensors measure only relative changes of pressure and recognize the direction of the change.

The instrumentation system for the discussed sensor relies on a coherence-addressing principle [13] to read out a phase shift between two polarizing modes in the sensing side-hole fiber. The phase shift $\Delta\phi_{SH}$ depends linearly on pressure as well as on temperature change

$$\Delta\phi_{SH} = (K_p \cdot \Delta p + K_T \cdot \Delta T) \cdot L_{SH} + \Delta\phi_0 \quad (6)$$

where p and T indicate, respectively, pressure and temperature acting on the fiber; $L_{SH} = 0.133$ m is the length of the side-hole fiber; and $\Delta\phi_0$ is the phase shift associated with the initial imbalance of the sensor. The sensitivity of the side-hole fiber to pressure and temperature is equal to $K_P = -13.3$ rad \cdot bar $^{-1}$ m $^{-1}$ and $K_T = -0.71$ rad \cdot $^{\circ}$ C $^{-1}$ m $^{-1}$, respectively. The system is composed of sensing and decoding interferometers with matched optical path delays (see Fig. 5), which makes it possible to place the sensor's head even a few kilometers away

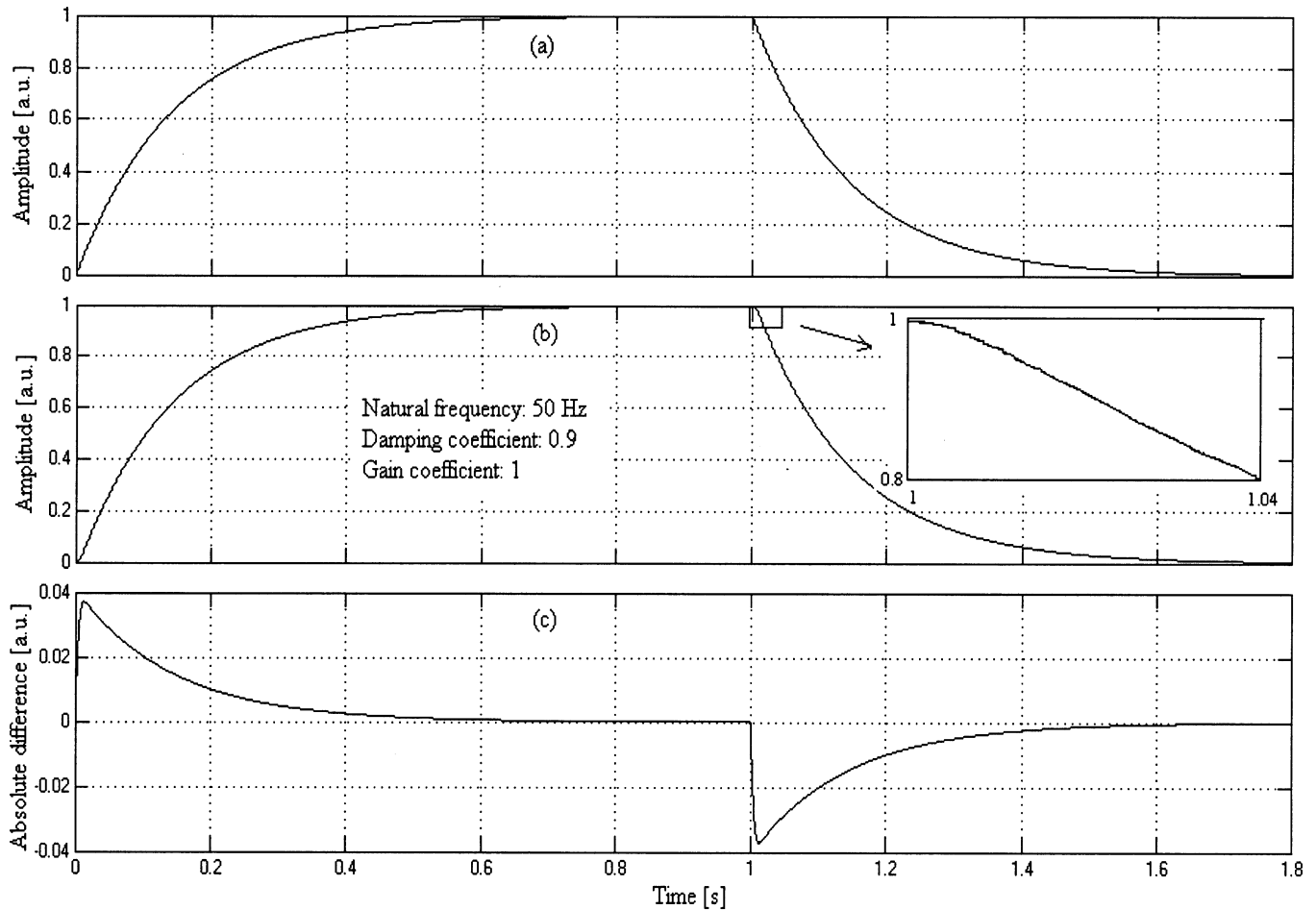


Fig. 3. Theoretical response of the second-order transducer to the exponential function. (a) Input rise and drop for a time constant of 200 ms. (b) Response of the transducer with a natural frequency of 50 Hz, damping and gain coefficient equal to 0.9 and 1, respectively. (c) Absolute difference between the input function and the transducer's response.

from the decoding system. The sensing interferometer is composed of the side-hole fiber, whereas a quartz-crystalline plate with an analyzer is employed as a decoding interferometer. The system is powered by a low-coherence superluminescent diode ($\lambda_0 = 809$ nm, $\Delta\lambda = 20$ nm), which is pigtailed with polarizing fiber. Linearly polarized light from the polarizing fiber is coupled by a polarization maintaining connector into one mode of the lead-in polarization maintaining fiber. The lead-in fiber and the side-hole fiber are spliced to each other with rotation of their polarization axes by $\pi/4$. This process assures an excitation of two polarization modes with equal amplitudes in the side-hole fiber. The signal of the side-hole fiber is connected with the decoding interferometer by the lead-out polarization maintaining fiber, which is aligned at $\pi/4$ angles with respect to the side-hole fiber and the polarization axes of the quartz-crystalline plate. The analyzer is also aligned at the $\pi/4$ angle with respect to the retardation plate. Such alignment assures maximum visibility of the interference fringes equal to 0.5 [14]. The interference signal is detected if the group imbalance ΔR_{SH} introduced by the side-hole fiber is compensated by the group imbalance ΔR_R introduced by the retardation plate

$$\Delta N_{SH} \cdot L_{SH} = \pm \Delta N_R \cdot d_R \quad (7)$$

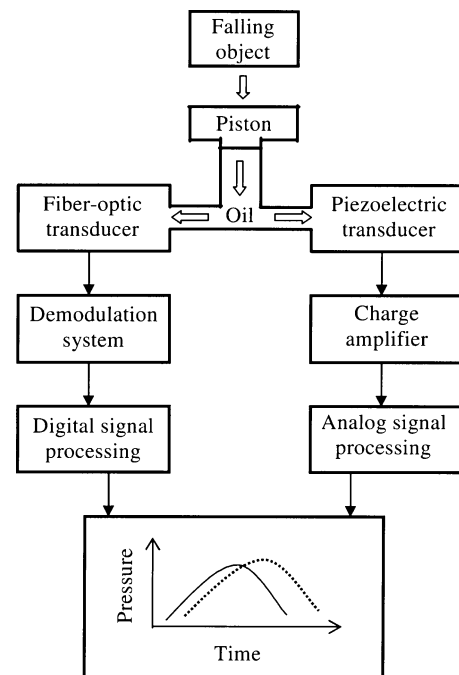


Fig. 4. Scheme of the system for dynamic calibration of the fiber-optic pressure sensor.

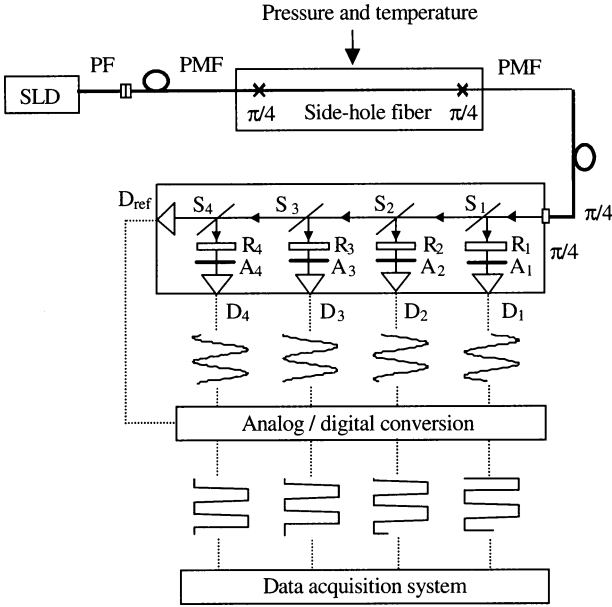


Fig. 5. Fiber-optic pressure sensor with a digital demodulation system. SLD: Superluminescent diode. PF: Polarizing fiber. PMF: Polarization maintaining fiber. S_{1-4} : Beam splitters. R_{1-4} : Retardation plates. A_{1-4} : Analyzers. D_{1-4} , D_{ref} : Pin photodiodes.

where ΔN_{SH} and ΔN_R are the group refraction indexes of the side-hole fiber and the retardation plate, respectively, whereas d_R is the thickness of the plate.

We used a digital demodulation system to read out the phase shift associated with the pressure changes [5]. The system contains four channels for decoding the interference signal and one reference channel for monitoring an average intensity at the sensor output. The plates are tilted to introduce the initial phase shift $\Delta\phi_R$ of the interference signal differing by $\pi/4$ in consecutive decoding channels, which, thus, allows unambiguous measurement of a phase shift with a resolution of one-eighth interference fringe in a dynamic range of 45 fringes. The intensity registered in the i th detection channel contains the information about the phase shift $\Delta\phi_{SH}$ induced in the side-hole fiber and is represented by the following equation:

$$I_i = I_0 \left[1 + 0.5\gamma(\Delta R_{SH} \pm R_R) \sin(\Delta\phi_{SH} \pm \Delta\phi_R^i) \right], \quad i = 1, 2, 3, 4 \quad (8)$$

where I_0 is the average light intensity at the system output and γ is the coherence function of the light source. Sinusoidal changes of intensity are registered in the detection channels and converted into digital TTL signals in such a way that a high level is generated when the interference signal is higher than the average intensity I_0 and a low level is generated for I_i lower than I_0 . The digital pulses are counted by the data acquisition system with a sampling rate up to 200 kHz and then converted into pressure values.

In the piezoelectric sensor, a measured pressure acts on a diaphragm that converts the pressure to a proportional force. The force is transferred to the quartz packet, which produces an electrical charge proportional to the pressure change. The electrical charge is converted into a voltage by a charge amplifier, and the voltage is read by the data-acquisition system with a resolution

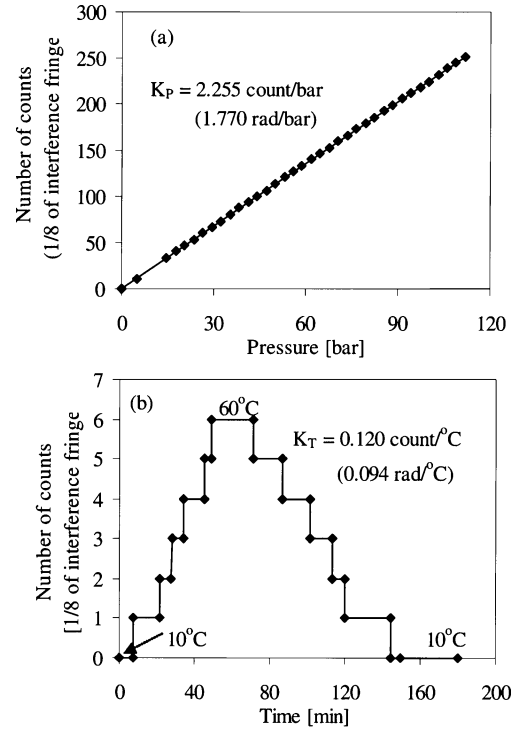


Fig. 6. Static calibration of the fiber-optic sensor. (a) Its pressure calibration curve and (b) response to temperature changes from 10 °C to 60 °C.

nine times higher than that of the tested sensor (0.05 bar for the reference sensor and 0.44 bar for the fiber-optic sensor in a range of 110 bar). The factory calibrated reference sensor measures dynamic pressure with a precision of 0.2% of full scale (FS) in a range from 0 to 250 bar, and its natural frequency is equal to 45 kHz.

IV. CALIBRATION RESULTS

We applied a static calibration procedure to initially determine the pressure and temperature sensitivity of the fiber-optic sensor, which made it possible to avoid resonance phenomena that occur during rapid pressure changes, but at the same time to determine precisely the static parameters of the sensor.

We determined the pressure sensitivity of the fiber-optic sensor from atmospheric pressure to 112 bar with a precision of 0.1% using the primary static-pressure dead-weight standard HARWOOD DWT-35KG. The calibration curve shown in Fig. 6(a) is characterized by very good linearity with the correlation coefficient equal to 1 and the sensitivity to pressure equal to 1.770 rad/bar. In our sensor, the operating range up to 112 bar is limited by vanishing birefringence in the side-hole fibers, which we recognized by irregularities in the shape of interference fringes in the decoding channels when pressure higher than 112 bar was applied. Because of the vanishing birefringence, only 70% of the full dynamic range of the sensing system (limited by the coherence length of the light source) is exploited.

To determine thermal stability, we measured the temperature phase shift of the sensor using the temperature stabilizer HAAKE C in a range from 10 °C to 60 °C with a precision of 0.1 °C [see Fig. 6(b)]. The pressure-to-temperature sensitivity

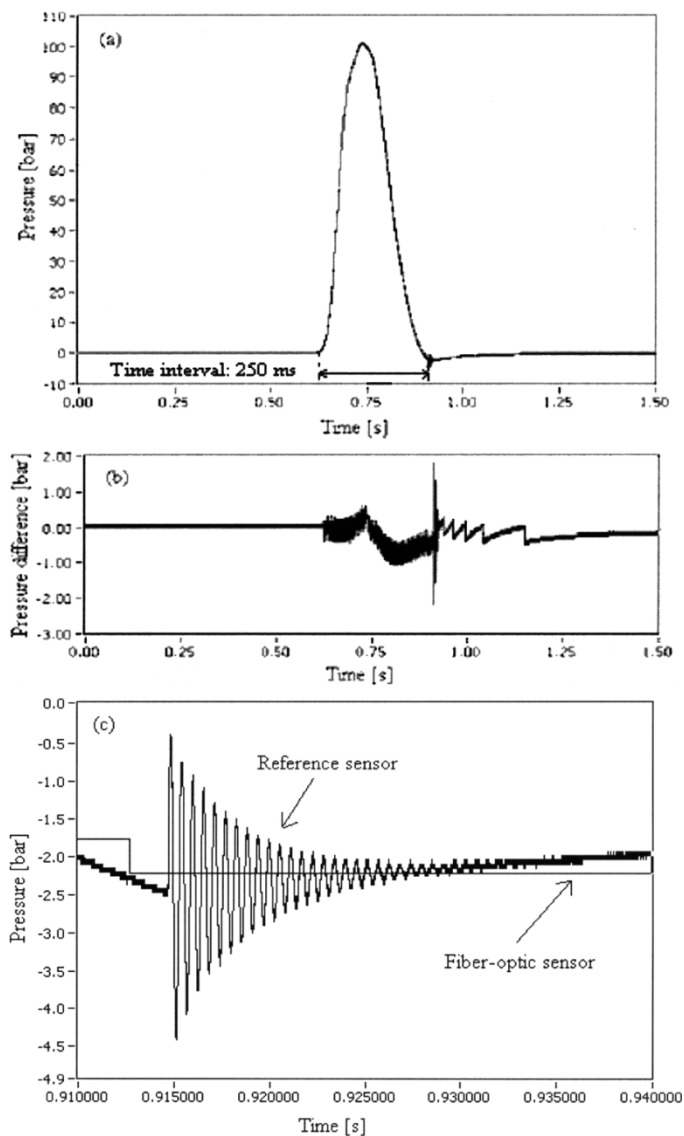


Fig. 7. Dynamic calibration of the fiber-optic sensor. (a) Responses of the tested fiber-optic sensor and reference piezoelectric sensor to the half-sine pressure pulse of a time interval of 250 ms. (b) Absolute difference between the readings of the two sensors. (c) Oscillations of a frequency equal to 1.8 kHz in the reference sensor.

ratio of the sensor is $19\text{ }^{\circ}\text{C}/\text{bar}$. The temperature change equal to $8.3\text{ }^{\circ}\text{C}$ corresponds to the resolution of the sensor, and this value is in line with the temperature change associated with the compression and decompression during rapid pressure changes. The additional phase shift caused by this uncontrolled temperature change could introduce an additional worst-case error of 0.8% FS. Nevertheless, a pressure sensor with such residual temperature sensitivity is suitable for many technical applications.

We compared the dynamic characteristics of the fiber-optic sensor with the calibrated piezoelectric sensor, which can be considered as a dynamic secondary standard. In Fig. 7(a), we show the responses of the two sensors to a half-sine pulse of a time interval equal to 250 ms and an amplitude equal to 101 bar. The maximum absolute difference between the sensor readings (excluding resonance oscillations of the reference sensor) is equal to 1.06 bar, which corresponds to 0.96% FS [see Fig. 7(b)]. In this measurement, no resonance oscillations

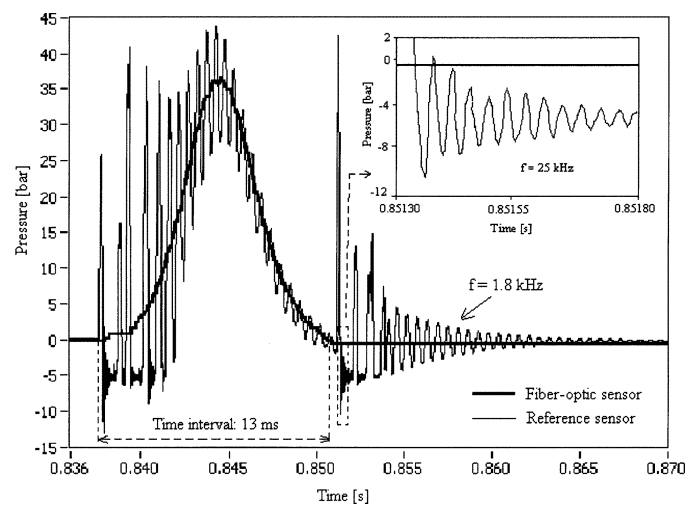


Fig. 8. Responses of the fiber-optic sensor and piezoelectric sensor to the half-sine pressure pulse of a time interval of 13 ms shows oscillations of a frequency of 1.8 and 25 kHz in the reference sensor.

occur in the fiber-optic sensor, whereas slight oscillations of a frequency equal to 1.8 kHz appear in the reference sensor [see Fig. 7(c)]. This result is due to the existence of a tube-shaped setup connecting both sensors and the pressure generator. Because of this, the diaphragm of the piezoelectric sensor with the tube represents a spring-mass oscillator with a natural frequency lower than the natural frequency of the sensor itself, depending on the tube dimensions and on the properties of the medium (in this case, oil). The damping factor is of the order of 10^{-2} in the piezoelectric sensor. The construction of the fiber-optic pressure sensor makes possible the use of a pressurized oil that will spread out in eight different directions and act simultaneously on as many points of the sensing fiber loop in the whole volume of the head which, thus, reduces undesirable oscillations. For time intervals greater than 400 ms, no resonance oscillations occur in either the fiber-optic sensor or the piezoelectric sensor. In Fig. 8, we show the response of the sensors to a half-sine pulse with a time interval equal to 13 ms. In the piezoelectric sensor, high-amplitude oscillations of a frequency equal to 1.8 kHz occur, whereas in the fiber-optic sensor, only phase-shifted slight oscillations of the same frequency take place. The slight oscillations are probably carried from the tube to the fiber-optic sensor during the resonance. This result shows that the construction of the fiber-optic sensor allows it to operate at frequencies about one order higher than the piezoelectric sensor. We also noticed that the reference sensor reads additional oscillations at the frequency equal to 25 kHz, which are excited by high-amplitude oscillations of 1.8 kHz. In Fig. 9, we show the response of the sensors to the linear pressure change of a slope equal to 224 bar/s, which was obtained from the KISTLER pressure generator by slow pressing the drop-weight. In this measurement, neither sensor detected noticeable oscillations. The maximum absolute difference between the sensor readings is equal to 0.55 bar, which corresponds to 0.50% FS [see Fig. 9(b)]. We also tested the sensor's response to the exponential decay of pressure from 90 bar to atmospheric pressure, with the relaxation time equal to 200 ms, which is shown in Fig. 10. The maximum absolute

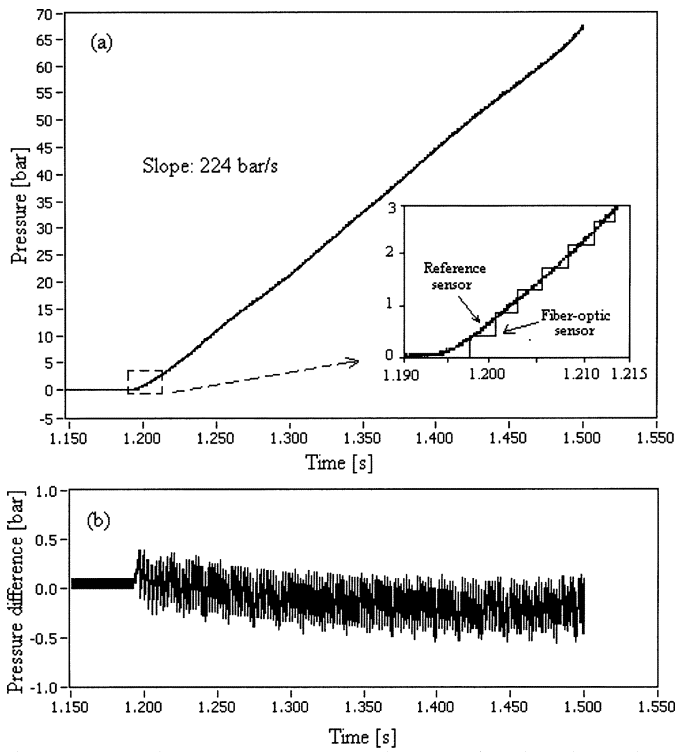


Fig. 9. Dynamic calibration of the fiber-optic sensor. (a) Responses of the fiber-optic sensor and piezoelectric sensor to linear pressure change of a slope of 224 bar/s. (b) Absolute difference between the readings of the two sensors.

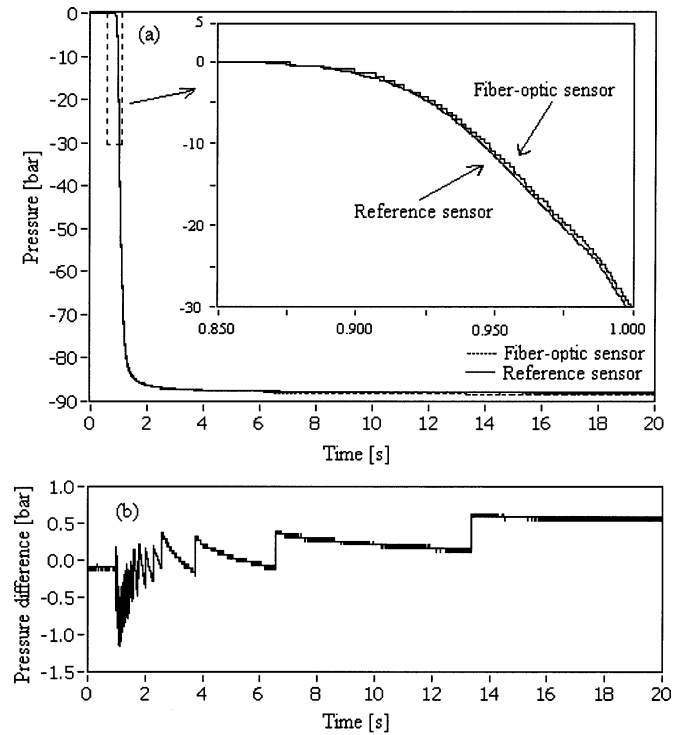


Fig. 10. Dynamic calibration of the fiber-optic sensor. (a) Responses of the fiber-optic sensor and piezoelectric sensor to exponential pressure change for a time constant of 200 ms. (b) The absolute difference between the readings of the two sensors.

difference between the readings of the two sensors is equal to 1.18 bar, which corresponds to 1.07% FS [see Fig. 10(b)]. This pressure change was obtained by quickly opening the

TABLE I
MAXIMUM DIFFERENCES BETWEEN READINGS OF THE FIBER-OPTIC SENSOR AND THE CALIBRATED PIEZOELECTRIC SENSOR FOR DIFFERENT PRESSURE CHANGE FUNCTIONS APPLIED FOR DYNAMIC CALIBRATION

Pressure change parameters	Maximum difference between sensor readings [% FS]
Half-sine pulse, time interval 250 ms	0.96
Linear, slope 224 bar/s	0.50
Exponential decay, relaxation time 200 ms	1.07

valve of the primary static-pressure dead-weight standard HARWOOD DWT-35KG. Compared with the measurements with the drop-weight pressure generator, this response shows a higher damping factor (of the order of 10^{-1}) and a lower natural frequency (of the order of 10^{-1} Hz), which is due to the long and curved pipes connecting the sensors with the static-pressure generator.

The results of the above comparison are set out in Table I. The various responses of the fiber-optic sensor show good agreement with those of the calibrated piezoelectric sensor if no resonance occurs. The maximum difference between readings of the two sensors is about 1% FS and is mainly caused by temperature changes during compression and decompression processes and a slight phase lag in the fiber-optic sensor response as a result of the longer fluid flow between the pressure generator and the fiber loop.

The responses of the sensors closely resemble the theoretical behavior of the second-order transducer. The discrepancies between the experimental and the calculated signal occur due to the curved flow of a liquid between the pressure generator and the sensors, irregularities in the tubes' radii, less than ideal shapes of the load pressure function, and temperature change during compression and decompression processes.

V. CONCLUSION

We presented the dynamic calibration of the fiber-optic pressure sensor based on birefringent side-hole fibers. Considering that the optical sensor will likely be applied in different measurement situations, we tested it in the static as well as in the dynamic regime of operation. We determined its pressure sensitivity using the primary static-pressure dead-weight standard. Next we compared the characteristics of the fiber-optic sensor with the responses of a calibrated piezoelectric dynamic pressure sensor (considered as a secondary dynamic pressure standard) for half-sine, linear, and exponential pressure change. The characteristics of the fiber-optic sensor are in good agreement with those of the reference piezoelectric sensor for the linear and exponential functions and for the half-sine when the pulse is wider than 400 ms. However, for half-sine pulses narrower than 250 ms, oscillations of the frequencies equal to 1.8 kHz occur in the piezoelectric sensor, which is due to the tube-shape setup connecting the two sensors with the pressure generator that causes the diaphragm of the piezoelectric sensor with the

tube to function as a spring-mass oscillator. Construction of the fiber-optic sensor reduces the undesirable oscillations, which thereby makes it possible to operate on frequencies higher by about one order than in the case of the piezoelectric sensor. Furthermore, the fiber-optic sensor described here allows measurement of static pressures. This promising capability of fiber-optic sensors should be further investigated; they indeed should be considered as secondary standards for both static and dynamic pressure measurements, which are better than commonly accepted piezoelectric reference transducers.

REFERENCES

- [1] A. N. Chester, S. Martellucci, and A. M. Verga Scheggi, *Optical Fiber Sensors*. Boston, MA: Martinus Nijhoff, 1987.
- [2] J. Dakin and B. Culshaw, *Optical Fiber Sensors*. Boston, MA: Artech House, 1997.
- [3] "Dynamic measurement of pressure—A literature survey," SP Swedish National Testing and Research Institute, J. Hjelmgren. [Online]. Available: http://www.sp.se/metrology/dynamic/dokument/2002_34.pdf
- [4] W. N. MacPherson, J. M. Kilpatrick, J. S. Barton, and J. D. C. Jones, "Miniature fiber optic pressure sensor for turbomachinery applications," *Rev. Sci. Instrum.*, vol. 70, pp. 1868–1874, 1999.
- [5] W. Urbanczyk, M. S. Nawrocka, and W. J. Bock, "Digital demodulation system for low-coherence interferometric sensors based on highly birefringent fibers," *Appl. Opt.*, vol. 40, pp. 6618–6625, 2001.
- [6] W. J. Bock, M. S. Nawrocka, and W. Urbanczyk, "Highly sensitive fiber-optic sensor for dynamic pressure measurements," *IEEE Trans. Instrum. Meas.*, vol. 50, no. 5, pp. 1085–1088, Oct. 2001.
- [7] J. P. Dakin and C. A. Wade, "Compensated polarimetric sensor using polarization-maintaining fiber in a differential configuration," *Electron. Lett.*, vol. 20, pp. 51–53, 1984.
- [8] W. J. Bock, M. S. Nawrocka, and W. Urbanczyk, "Studies of temperature-insensitive dynamic pressure sensing using elliptical-core side-hole fibers," in *Proc. SPIE Applications on Photonic Technology 6*, vol. 5260, R. A. Lessard and G. A. Lampropoulos, Eds., Bellingham, WA, 2003, pp. 278–283.
- [9] H. M. Xie, P. Dabkiewicz, R. Ulrich, and K. Okamoto, "Side-hole fiber for fiber-optic pressure sensing," *Opt. Lett.*, vol. 11, pp. 333–335, 1986.
- [10] M. S. Nawrocka and W. Urbanczyk, "Optimization of detection system for low-coherence interferometric sensors based on highly birefringent fibers," *Opt. Appl.*, vol. 31, pp. 231–250, 2001.
- [11] M. N. Charasee, M. Turpin, and J. P. Le Pesant, "Dynamic pressure sensing with a side-hole birefringent optical fiber," *Opt. Lett.*, vol. 16, pp. 1043–1045, 1991.
- [12] L. Meirovitch, *Elements of Vibration Analysis*. New York: McGraw-Hill, 1986.
- [13] S. A. Al-Chalabi, B. Culshaw, and D. E. N. Davies, "Partially coherent sources in interferometric sensors," in *Proc. IEEE 1st Int. Conf. Optical Fiber Sensors*, London, U.K., 1983, pp. 132–135.
- [14] W. Urbanczyk, P. Kurzynowski, W. A. Wozniak, and W. J. Bock, "Performance analysis for temperature-compensated white-light interferometric fiber sensors," *Optik*, vol. 4, pp. 153–158, 1997.

Magdalena S. Nawrocka received the M.S. degree in electronics and telecommunications with specialization in fiber optics and the Ph.D. degree in physics from the Wrocław University of Technology, Wrocław, Poland, in 1996 and 2001, respectively.

She was awarded the NATO Science Fellowship in 2001 by the Natural Sciences and Engineering Research Council of Canada and was with the Université du Québec en Outaouais, Québec, QC, Canada, working on fiber-optic sensors for dynamic pressure and temperature measurements. She is currently a Visiting Scientist with the Nanophotonics and Nanofabrication Research Group, Florida International University, Miami, where her research includes nanophotonic sensors. She has authored and co-authored 20 scientific papers in the field of fiber optics.

Wojtek J. Bock (M'85–F'03) received the M.Sc. degree in electrical engineering and the Ph.D. degree in solid state physics from the Warsaw University of Technology, Warsaw, Poland, in 1971 and 1980, respectively.

He is currently a Full Professor of electrical engineering and Canada Research Chair in photonics with the Université du Québec en Outaouais, Québec, QC, Canada. He is also Director of the Photonics Research Center at this University. His research interests include fiber-optic sensors and devices, multisensor systems, and precise measurement systems of nonelectric quantities. He has authored and co-authored more than 200 scientific papers, patents, and conference papers in the fields of fiber optics and metrology.

Dr. Bock is a member of the Administrative Committee of the IEEE Instrumentation and Measurement Society. In May 1997, he was General Chairman of the IMTC/97 in Ottawa, ON, Canada.

Waclaw Urbanczyk, photograph and biography not available at the time of publication.